Journal of Biomedical Optics

BiomedicalOptics.SPIEDigitalLibrary.org

Third-harmonic generation susceptibility spectroscopy in free fatty acids

Yu-Cheng Chen
Hsun-Chia Hsu
Chien-Ming Lee
Chi-Kuang Sun

SPIE.

Third-harmonic generation susceptibility spectroscopy in free fatty acids

Yu-Cheng Chen,[a] Hsun-Chia Hsu,[a,b] Chien-Ming Lee,[c] and Chi-Kuang Sun[a,c,d,*]
[a]National Taiwan University, Molecular Imaging Center, Taipei 10617, Taiwan
[b]Washington University in Saint Louis, Department of Biomedical Engineering, Saint Louis, Missouri 63130, United States
[c]National Taiwan University, Department of Electrical Engineering and Graduate Institute of Photonics and Optoelectronics, Taipei 10617, Taiwan
[d]Institute of Physics and Research Center for Applied Sciences, Academia Sinica, Taipei 11529, Taiwan

Abstract. Lipid-correlated disease such as atherosclerosis has been an important medical research topic for decades. Many new microscopic imaging techniques such as coherent anti-Stokes Raman scattering and third-harmonic generation (THG) microscopy were verified to have the capability to target lipids *in vivo*. In the case of THG microscopy, biological cell membranes and lipid bodies in cells and tissues have been shown as good sources of contrast with a laser excitation wavelength around 1200 nm. We report the THG excitation spectroscopy study of two pure free fatty acids including oleic acid and linoleic acid from 1090 to 1330 nm. Different pure fatty acids presented slightly-different THG $\chi^{(3)}$ spectra. The measured peak values of THG third-order susceptibility $\chi^{(3)}$ in both fatty acids were surprisingly found not to match completely with the resonant absorption wavelengths around 1190 to 1210 nm, suggesting possible wavelengths selection for enhanced THG imaging of lipids while avoiding laser light absorption. Along with the recent advancement in THG imaging, this new window between 1240 to 1290 nm may offer tremendous new opportunities for sensitive label-free lipid imaging in biological tissues. [DOI: 10.1117/1.JBO.20.9.095013]

Keywords: third-harmonic generation; free fatty acids; oleic acid; linoleic acid; third-order susceptibility; ultrafast spectroscopy.

Paper 150381R received Jun. 4, 2015; accepted for publication Aug. 25, 2015; published online Sep. 25, 2015.

1 Introduction

Lipids are one of the most significant components in our body, forming cell membranes, neural myelin sheaths, and stratum corneum of the skin. However, there are also lipid-related diseases causing great attention in the medical community. Especially in epidemiology, atherosclerosis is considered the leading cause for cardiovascular disease (CVD) contributing to high mortality worldwide. For advanced investigation and monitoring of CVD, *in vivo* label-free imaging of lipids has become one of the primary topics for the development of new imaging techniques. Recently, third-harmonic generation (THG) microscopy[1–10] and coherent anti-Stokes Raman scattering (CARS) microscopy[11–15] have been shown to be capable of imaging lipid content biological structures and have been widely applied to image cell membranes, hepatocytes, red blood cells, adipocytes, brain tissues, and even atherosclerotic plaques.[15–19] Compared to CARS microscopy that has been a useful tool for biological imaging and identification of CH_2 stretch and C=O bands near 3000 nm,[11–15] THG microscopy is expected to possess the unique capability to image and identify C–H second overtones, with which most biological lipid bodies are in abundance. A number of novel and promising physical characteristics have been investigated for lipids and mixed oils.[16,20] However, one critical characteristic, which has been the subject of only a few experimental studies, is the nonlinear optical properties of pure fatty acids.

Previous THG imaging studies indicated that THG can provide rich contrast for lipids,[2,10] when excited with a laser wavelength around 1200 nm,[2–4] which may be possibly attributed to the resonant enhancement with the second overtone and combination absorption bands of lipids. However, a detailed spectroscopic study on the origin of this THG contrast is missing. In general, the fundamental wavelength for THG excitation in previous papers was chosen to be within the range of 1200 to 1300 nm for deep tissue imaging with reduced scattering and to avoid strong water absorption.[21,22] In this paper, we report a spectroscopy study for the third-order susceptibility $\chi^{(3)}$ of THG in two different free fatty acids, oleic acid (OA) and linoleic acid (LA), between 1090 and 1330 nm. By comparing the measured THG $\chi^{(3)}$ spectra with their corresponding absorption spectra, experimental results demonstrate that both types of fatty acids appear to have relatively higher third-order susceptibility $\chi^{(3)}$ between 1240 to 1280 nm, differing from the strong absorbance peak around 1210 nm. This paper represents the only study to examine the third-order nonlinear susceptibility $\chi^{(3)}$ of THG in pure lipids (free fatty acids), and will provide unique spectral information of free fatty acids while opening up a new wavelength window for future THG lipid imaging without resonant absorption.

2 Methods and Materials

2.1 *Sample Preparation*

Two types of common yet essential free unsaturated fatty acids, OA and LA (Sigma-Aldrich), were examined in this study due to their importance for maintaining our health. An unsaturated dietary lifestyle, including monounsaturated and

*Address all correspondence to: Chi-Kuang Sun, E-mail: sun@ntu.edu.tw

1083-3668/2015/$25.00 © 2015 SPIE

polyunsaturated fatty acids (MUFAs, PUFAs), can help reduce the risk of heart disease by raising levels of high-density lipoprotein in the blood, and by supporting the functioning of cells and normal cellular activity.[23] In addition to OA and LA, for reference we also measured the THG signals of pure water (Millipore Corp.) and bare fused-silica substrate (UQG Optics Ltd., Vitreosil® Grade077, thickness 0.17 mm, transparent window 260 to 2000 nm). All liquid samples were carefully dripped on clean, polished fused-silica substrates with each droplet controlled within 10 μl. Moreover, the whole microscope stage was sealed (isolated) in a low-oxygen space to prevent oxidation from air exposure. In addition, we carefully controlled the amount of each solution so as to maintain an equivalent thickness (0.12 mm) of all droplet samples as much as possible.

2.2 *Setup and Measurement of Third-Harmonic Generation Images*

Figures 1(a) and 1(b) show the schematic diagram of the optical setup for THG image acquisition. The frequency dependent third-order nonlinear susceptibility $\chi^{(3)}$ of THG was then analyzed from the acquired images. Our laser-scanning THG microscope was adapted with a commercialized Leica confocal microscopic system to collect the transmitted THG signals. The output of an optical parametric oscillator (OPO), which was pumped by a Ti: Sapphire femtosecond laser (Chameleon-Compact OPO, Coherent) and provided output wavelength from 1080 to 1500 nm, was coupled into the scanning system as the excitation source. We used a 2-mm-working-distance, high-numerical aperture, infrared objective (Leica/IR 20X/water/NA0.75) to focus the laser beam on the desired location of the droplet interface for THG microscopy and spectroscopy with a focused spot size close to its diffraction limit. The average laser power after the objective for all output wavelengths was fixed to be 30 mW. Finally, the forward-propagating THG signals were collected by a condenser and guided through a color glass filter (CG-BG 40, Schott, Germany) and a narrow bandpass filter into a photomultiplier tube (PMT). For comparison of the wavelength-dependent THG intensities at the sample-air interface, all the settings and conditions were controlled to be exactly the same for different excitation wavelengths, including the PMT voltage, beam size, frame rate, and aperture size. In order to make fair comparisons between all samples, all interfacial THG intensities were measured at the exact same thickness (0.12 mm) according to selection of THG images. The THG intensity point on the individual $x-z$ profile was averaged by three acquisitions, then five points along the sample-air interface (along the x-axis direction as defined in Fig. 1) were randomly chosen and averaged to calculate the determined THG intensity. Note that the two-way wavelength scanning (both 1090 to 1300 nm and 1300 to 1090 nm) was used to confirm that the sample's chemical properties remain consistent during the acquisition of the whole spectrum.

2.3 *Calculation for Third-Harmonic Generation $\chi^{(3)}$*

In order to retrieve the third-order susceptibility value of THG in OA and LA, the THG intensity images of a standard, bare fused-silica substrate were also acquired as our reference for calibration [as plotted in Fig. 1(c)]. The third-order susceptibility value of THG in the reference fused-silica substrate

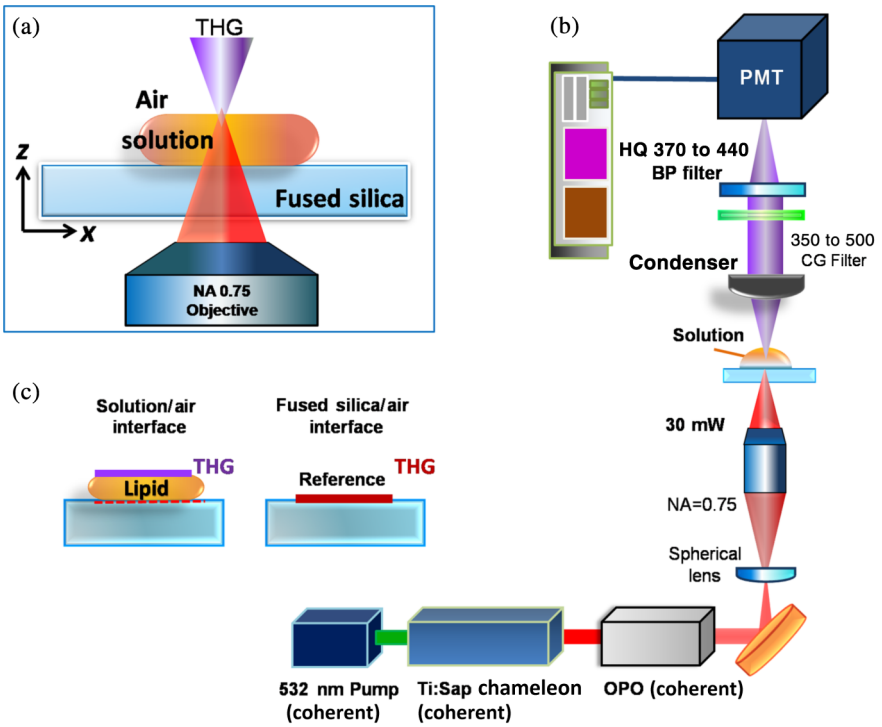

Fig. 1 Schematic diagram showing the optical setup for third-harmonic generation (THG) and intensity image acquisition: (a) the experimental setup for acquiring the THG signals at oil/air interfaces, (b) the optical system of the THG microscopy, and (c) enlarged diagram showing the THG signal acquisition from the two individual interfaces for $\chi^{(3)}$ calibration, which are the lipid/air interface and the fused-silica/air interface.

(1.94×10^{-22} m^2/V^2 at 1100 nm, 1.85×10^{-22} m^2/V^2 at 1200 nm, 1.77×10^{-22} m^2/V^2 at 1320 nm) was previously known.[24,25] We seek to derive the third-order susceptibility ratio of our lipid samples relative to this known fused-silica, [$\chi^{(3)}$ lipid/$\chi^{(3)}$ fused-silica], by measuring the ratio of the interfacial THG power from the air/lipid interface and air/fused-silica interfaces, respectively, that is, $I_{(3\omega)\text{lipid/air}}/I_{(3\omega)\text{fused-silica/air}}$. Therefore, the third-order susceptibility of lipid can be calibrated based on the interfacial THG power ratio of lipid/air to fused-silica/air. Note that we can ignore the focal spot size and the fundamental laser pulse width variation of OPO at different wavelengths, since we are only considering the THG ratio at respective wavelengths.

To calculate the $\chi^{(3)}$ of both fatty acids, the model of focused Gaussian beam was adopted.[26] A widely accepted analytical model was used[26–29] to estimate the relative THG $\chi^{(3)}$ value. Now, we consider a focused Gaussian beam propagating in the $+z$ direction and tightly focused right at the interface between air and lipid, the electric field of the fundamental wave E_ω can be expressed as[30]

$$E_\omega(x,y,z) = \frac{A_\omega}{\left(1+i\frac{z}{b}\right)} \exp\left[-\frac{x^2+y^2}{w_{\omega 0}^2\left(1+i\frac{z}{b}\right)}\right], \tag{1}$$

where A_ω is related to field amplitude, w_0 is the beam waist of the fundamental beam, and the confocal parameter $2b$ is defined with $b = kw_0^2/2 = \pi n w_0^2/\lambda$. By following the THG derivation[31] with

$$P_{3\omega}^{NL}(3\omega) = \frac{1}{2^2}\varepsilon_0 \chi^{(3)} E_\omega^3, \tag{2}$$

where $\chi^{(3)}$ is the third-order nonlinear susceptibility for THG, the power of THG ($I_{3\omega}$) can be approximated as

$$I_{3\omega} \alpha I_\omega^3 |J_3|^2, \tag{3}$$

where the integral J_3 is defined as

$$J_3(\Delta k, z) = \int_{-\infty}^{z} \frac{\chi^{(3)}(z')}{\left(1+i\frac{z'}{b}\right)^2} e^{(i\Delta k z')} dz', \tag{4}$$

in which J_3 is the phase matching integral of THG under a tightly focused condition and $\Delta k = 3k(\omega) - k(3\omega)$ is the phase mismatch. By substituting the respective refractive indices $n_{\omega\text{air}}$, $n_{3\omega\text{lipid}}$, $n_{\omega\text{fs}}$, $n_{3\omega\text{fs}}$, $n_{\omega\text{air}}$, $n_{3\omega\text{air}}$,[32–34] the peak power of THG signal generated at the lipid/air interface ($I_{3\omega,\text{lipid/air}}$) and fused-silica/air interface ($I_{3\omega,\text{fs/air}}$) can be approximated as[29]

$$I_{3\omega,\text{lipid/air}} \propto I_\omega^3 |[J_{\text{lipid}}(-\infty, 0) + J_{\text{air}}(0, \infty)]|^2, \tag{5}$$

$$I_{3\omega,\text{fs/air}} \propto I_\omega^3 |[J_{\text{fused-silica}}(-\infty, 0) + J_{\text{air}}(0, \infty)]|^2. \tag{6}$$

Based on the experimented THG power ratio of the acquired air/lipid interface to air/fused-silica, along with the published susceptibilities of air and fused-silica, $\chi^{(3)}$ air (ω), $\chi^{(3)}$ fused-silica (ω) as our references,[25] the absolute value of the third-order susceptibility of lipid $\chi^{(3)}$ lipid (ω) can be then resolved. Moreover, the $\chi^{(3)}$ water (ω) of pure water in the same setup was measured and normalized following the same process as well.[20]

By following our normalization and calibration process to solve the collected respective interfacial THG signals from both interfaces, the third-order nonlinear susceptibility $\chi^{(3)}$ lipid (ω) data sets for OA and LA can be retrieved as plotted in Figs. 2(a) and 2(b), respectively. To illustrate the confidence level of the calibrated values, an error bar for each calculated THG $\chi^{(3)}$ value was calculated by considering the variations of the peak power of THG in all measurements (repeatability error). Additionally, we considered other potential sources of the calibration errors including the spectral transmission calibration error ($< \pm 2.5\%$), and the refractive index uncertainty of the adopted literature values ($< \pm 0.5\%$).

3 Results and Discussion

The calibrated THG $\chi^{(3)}$ spectra for OA and LA between 1090 and 1320 nm are shown in Figs. 2(a) and 2(b) as red and blue solid dots, respectively. According to our experimental results, the peak values of third-order susceptibility $\chi^{(3)}$ in OA and LA are approximately $3.21 \pm 0.33 \times 10^{-22}$ m^2/V^2 at 1260 nm, and $2.94 \pm 0.25 \times 10^{-22}$ m^2/V^2 at 1280 nm, respectively. For both acids, a 2 to 3 times higher value of $\chi^{(3)}$ can be found from 1240 to 1290 nm when compared with water.

Previous studies had shown that if one of the virtual levels is close to a real electronic (vibronic in this specific case) level, the third-order nonlinear susceptibility will be strongly enhanced so that an enhanced THG signal would be observed,[35–39] such as in melanin,[40] hemoglobin,[38] elastin,[6] nanoparticles,[41] and exogenous dyes.[37,39] In order to discuss the resonant effect, we present both the measured absorption spectra of the studied lipids together with the measured THG $\chi^{(3)}$ values in Fig. 2(c). In the inset of Fig. 2(c), we reproduce the schematic structure of a single OA ($C_{18}H_{34}O_2$) molecule and LA ($C_{18}H_{34}O_2$) molecule, respectively. According to previous studies, the appearance of the absorption peaks around 1180 to 1230 nm is quite typical in most biological oils,[22,42] which corresponds to the second overtone of C—H stretching vibration of various chemical groups (—CH2, —CH3, —CH=CH—). However, to our surprise, experimental results have shown that the maximum THG $\chi^{(3)}$ values of both fatty acids exist outside this expected absorption wavelength range (1180 to 1210 nm), which was claimed in previously published data on a mixed oil.[2,20] In other words, the measured THG $\chi^{(3)}$ spectra does not exactly follow the same wavelength-dependent trend as the linear absorption constant in both fatty acids. Previous works[1–10] have extensively used THG microscopy for imaging lipids near 1200 nm (1180 to 1230 nm) in order to match the second overtone; however, here we suggest that 1270 nm (1240 to 1290 nm) is a better window for THG imaging of lipids since both fatty acids displayed relative higher and stable $\chi^{(3)}$ values while excitation light absorption by lipids can be completely avoided. This conclusion does not agree completely with the expected single-photon resonant enhancement picture through the second overtone centered on 1210 nm. When excited with a wavelength close to the absorption peak at 1210 nm, a stronger THG signal was indeed observed, with more than those excited by shorter laser wavelengths, indicating the existence of the expected single-photon resonant enhancement effect. However, out of our expectation, the peak values of third-order susceptibility $\chi^{(3)}$ in OA and LA is located at 1260 and 1280 nm, respectively. For the wavelength range longer than 1210 nm, the THG $\chi^{(3)}$ value is no longer proportional to the absorption constant spectrally. The mechanism for this strong $\chi^{(3)}$ enhancement around

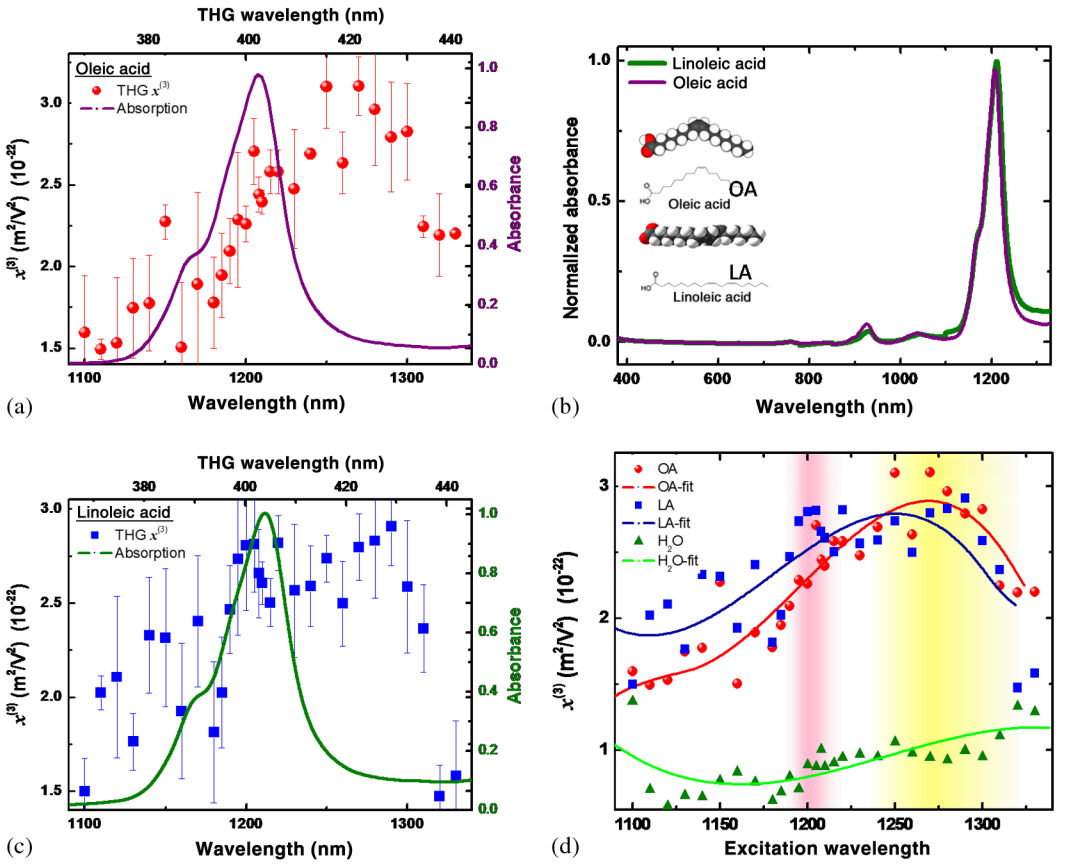

Fig. 2 Data sets for oleic acid (OA) and linoleic acid (LA) retrieved and plotted: (a) absorption spectrum (purple solid line) and calibrated THG third-order susceptibility (red solid dots) of OA, (b) absorption spectrum (green solid line) and calibrated THG third-order susceptibility (blue solid dots) of LA. The error bars are plotted in each corresponding measured data of $\chi^{(3)}$ values. Comparision of the absorption spectra (380 to 1320 nm) of both fatty acids: (c) OA shown as the purple curve and LA shown as the green curve. The molecular structures of OA and LA were also given in the inset. Comparison of the calibrated $\chi^{(3)}$ values: (d) OA (red dots), LA (blue dots), and pure water (green dots), while the fitting curves for THG spectra were also plotted in red, blue, and green solid lines, respectively. The pink background around 1180 to 1230 nm shows the original window in previous studies while the yellow region around 1240 to 1280 nm suggests a new window for future THG imaging of lipids.

1260 to 1280 nm needs further investigation. We have measured the absorption spectra of OA and LA to investigate the possible two-photon (around 630 to 640 nm) and three-photon (around 420 to 427 nm) resonances. As can be seen in Fig. 2(b), no measurable absorption around these multiphoton wavelengths can be observed, thus providing no evidence for multiphoton resonance effects. It is well-known that through third-order processes some single-photon-forbidden transitions can be probed (such as the stimulated Raman process).[43] One possible mechanism for this 1260 to 1280 nm peak is thus through the resonance with a single-photon dark state, which is instead resonanced through this nonlinear THG $\chi^{(3)}$ process. It is noted that this THG resonance at 1260 or 1280 nm is with a much broader bandwidth than the single-photon absorption peaked at 1210 nm, thus indicating a much shorter dephasing time of this unknown resonance state than the vibronic second overtone centered around 1210 nm. It is also important to state that the accuracy of our measurement relies on the correctness of the calibration source, which is the previously published third-order susceptibility value of THG in the reference fused-silica substrate.[24,25]

As plotted in Fig. 2(d), the curve fittings of OA and LA are elucidated as well. Combined with the known fact that the second overtone of C—H stretching modes of *cis* double bond is very close to 1200 nm in lipids,[42,44–45] similar $\chi^{(3)}$ values were found at that spectral regime in both fatty acids. Since both OA and LA have similar absorption spectra (also true for most oils), it is not that strange that the measured nonlinear third-order susceptibilities also share a similar trend in the spectral response. Despite the THG $\chi^{(3)}$ spectra of both fatty acids being alike, the maximum values of $\chi^{(3)}$ still correspond to different wavelengths. Interestingly, the values of LA is slightly larger than that of OA before 1210 nm, while the $\chi^{(3)}$ values of OA becomes larger than LA at longer wavelengths. In Fig. 3, we provide evidence showing the THG images of respective lipid/air interfaces under the excitation wavelengths at 1210 and 1280 nm. Apparently, both fatty acids show stronger interfacial THG intensities at 1280 than 1210 nm, demonstrating the excellent correlation between THG spectra and THG imaging. In chemical terms, OA is classified as a monounsaturated omega-9 fatty acid with a single *cis* double bond in the center (also the bending site), while LA is an omega-6 fatty acid with two *cis* double bonds located at the 9th and 12th carbon from the —OH end. Given that both fatty acids are similar in most properties, both lipids still vary in their molecular structures,

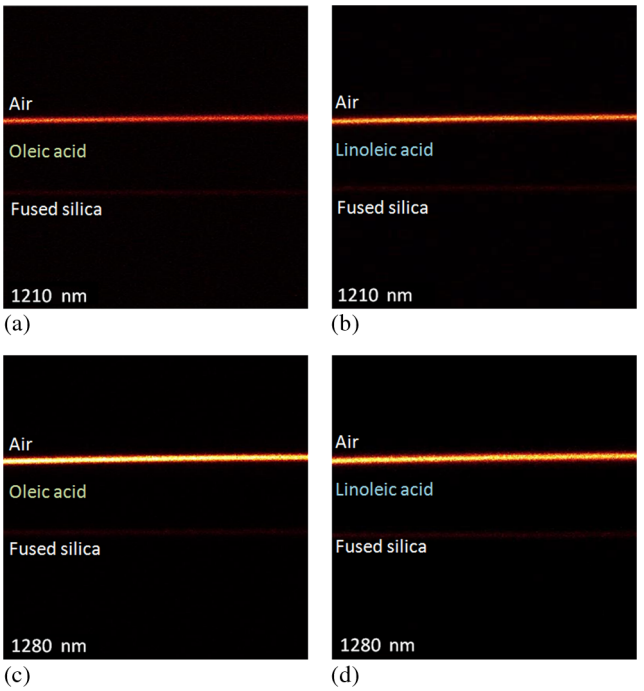

Fig. 3 THG images of the lipid/air interfaces under excitation wavelengths at 1210 and 1280 nm. Excited under 1210 nm: (a) oleic acid/air interface and (b) linoleic acid/air interface; excited under 1280 nm: (c) oleic acid/air interface and (d) linoleic acid/air interface. All images display the vertical section ($x-z$ plane) of each acquisition. Image size: 600 μm × 600 μm.

in which LA possesses a larger bending angle than OA resulting in a relatively higher degree of freedom of movement. This important result demonstrates that different pure lipids may not possess exactly the same THG $\chi^{(3)}$ values in all spectral regimes, therefore it is potentially possible for THG to spectrally distinguish different lipids. Our study also indicates the importance of selecting different THG excitation wavelengths in order to achieve the optimum THG efficiency of different fatty acids. Our results also imply the importance of characterizing the THG spectra of different triglycerides and cholesterols, which are the most abundant lipids in our body. Due to their high-scattering characteristics with a solid and opaque form at room temperature, our current methodology is not capable of characterizing accurately the THG spectra of different triglycerides and cholesterols.

The fact of different THG $\chi^{(3)}$ spectra for different free fatty acids implies the potential application of THG spectroscopy for quantitative composition analysis with near infrared (NIR) spectroscopy.[46] Conventional IR spectroscopy plays an important role in elucidation of molecular structures based on molecule-specific absorption spectra (such as fingerprint region) in the range about 1000 to 4000 cm^{-1}.[22] As for the NIR spectral range between 5000 to 10,000 cm^{-1} (1000 to 2000 nm wavelength), the absorption spectra of oils are composed of wide overlapping overtones and combinational bands.[22,40] With the benefit of computer and algorithm, chemometric methods such as principal component analysis and partial least square regression have shown success in quantitative composition analysis of mixed samples. NIR spectroscopy has now been applied to the prediction of the composition of edible lipids[47] as well as to the determination of the *trans* lipid content iodine value and the saponification number of edible lipids.[48,49] THG $\chi^{(3)}$ spectroscopy, however, has inherent advantages of subfemtoliter spatial specificity due to its local excitation nature. If specific calibrating chemometric algorithm for THG spectroscopy is available in the future, it will be a powerful technique for real-time quantitative composition analysis of lipids such as in atherosclerotic plaques. Taking advantage of the THG spectral selectivity of free fatty acids, it is also possible to develop THG microscopy as a label-free bond-selective imaging tool.[50] Combined with the statistical analysis tools analogous to that used in NIR spectroscopy, we believe that there is great potential for single-laser-beam-based THG spectroscopic imaging to be applied to analyze lipid compositions or structures pixel by pixel as being demonstrated by CARS microspectroscopy.[51,52] THG is also interface-sensitive[53] which makes THG spectroscopy an appropriate technique with a strong contrast to study the mechanism of atherosclerotic plaques occurring in the surface of artery vessels. In addition to composition analysis of lipids, through combining with the polarized THG imaging method[54,55] and spectral analysis,[56] molecular ordering of lipid structures might also be revealed.

4 Conclusions

In summary, our study aims to calibrate and provide the THG $\chi^{(3)}$ values of pure fatty acids in the NIR regime between 1090 to 1330 nm. Here we report the THG excitation spectrum study of two representative free fatty acids including OA and LA. It has been well believed that the rich CH_2 bonds in lipid molecules may contribute a strong vibrational second overtone near 1210 nm and enhance the THG spectrum. As we expected, in free fatty acids our results show that the THG third-order susceptibility $\chi^{(3)}$ peaks near 1240 to 1280 nm. This spectral characteristic suggests that there are factors other than single-photon-resonance through the originally expected second overtone contribute to the enhanced THG $\chi^{(3)}$ values of OA and LA (free fatty acids) in our studied spectral range. Our results suggest that 1270 nm (1240 to 1290 nm) may be a better window for THG imaging of lipids since both fatty acids displayed relatively higher and stable $\chi^{(3)}$ values while excitation light absorption by lipids can be completely avoided. Moreover, our results imply that pure fatty acids may have different $\chi^{(3)}$ values at different spectral regime, in which OA presented higher $\chi^{(3)}$ values at longer wavelengths and vice versa. Our research not only provides new spectral information for the choice of the laser excitation wavelength for future noninvasive THG imaging, but also suggests a potential method for THG microspectroscopy and bond-selective imaging in lipid-correlated diseases.

Acknowledgments

The authors acknowledge the financial support of Ministry of Science and Technology of Taiwan as well as National Health Research Institute under NHRI EX101-9936EI. The authors also would like to acknowledge Li-Chyong Chen of the Center for Condensed Matter Sciences, National Taiwan University for her technical support.

References

1. C. S. Hsieh et al., "Higher harmonic generation microscopy of in vitro cultured mammal oocytes and embryos," *Opt. Express* **16**, 11574–11588 (2008).
2. D. Débarre et al., "Imaging lipid bodies in cells and tissues using third-harmonic generation microscopy," *Nat. Methods* **3**, 47–53 (2006).

3. S. Y. Chen, H. Y. Wu, and C. K. Sun, "In vivo harmonic generation biopsy of human skin," *J. Biomed. Opt.* **14**(6), 060505 (2009).
4. C. K. Sun et al., "Higher harmonic generation microscopy for developmental biology," *J. Struct. Biol.* **147**(1), 19–30 (2004).
5. S. P. Tai et al., "In vivo optical biopsy of hamster oral cavity with epi-third-harmonic-generation microscopy," *Opt. Express* **14**(13), 6178–6187 (2006).
6. C. H. Yu et al., "In vivo and ex vivo imaging of intra-tissue elastic fibers using third-harmonic-generation microscopy," *Opt. Express* **15**(18), 11167–11177 (2007).
7. J. H. Lee et al., "Noninvasive in vitro and in vivo assessment of epidermal hyperkeratosis and dermal fibrosis in atopic dermatitis," *J. Biomed. Opt.* **14**(1), 014008 (2009).
8. S. Y. Chen et al., "Infrared-based third and second harmonic generation imaging of cornea," *J. Biomed. Opt.* **14**(4), 044012 (2009).
9. M. R. Tsai et al., "In vivo optical virtual biopsy of human oral mucosa with harmonic generation microscopy," *Biomed. Opt. Express* **2**(8), 2317–2328 (2011).
10. C. K. Tsai et al., "Virtual optical biopsy of human adipocytes with third harmonic generation microscopy," *Biomed. Opt. Express* **4**, 178–186 (2013).
11. T. T. Le, S. Yue, and J. X. Cheng, "Shedding new light on lipid biology with coherent anti-Stokes Raman scattering microscopy," *J. Lipid Res.* **51**(11), 3091–3102 (2010).
12. T. T. Le, T. B. Huff, and J. X. Cheng, "Coherent anti-Stokes Raman scattering imaging of lipids in cancer metastasis," *BMC Cancer* **9**(1), 42 (2009).
13. C. Heinrich et al., "Selective imaging of saturated and unsaturated lipids by wide-field CARS-microscopy," *Opt. Express* **16**, 2699–2708 (2008).
14. Y. Yi et al., "Lipid droplet pattern and nondroplet-like structure in two fat mutants of caenorhabditis elegans revealed by coherent anti-Stokes Raman scattering microscopy," *J. Biomed. Opt.* **19**(1), 011011 (2014).
15. M. C. Potcoava et al., "Raman and coherent anti-Stokes Raman scattering microscopy studies of changes in lipid content and composition in hormone-treated breast and prostate cancer cells," *J. Biomed. Opt.* **19**(11), 111605 (2014).
16. H. W. Wang et al., "Imaging and quantitative analysis of atherosclerotic lesions by CARS-based multimodal nonlinear optical microscopy," *Arterioscler. Thromb. Vasc. Biol.* **29**(9), 1342–1348 (2009).
17. J. X. Cheng et al., "Ordering of water molecules between phospholipid bilayers visualized by coherent anti-Stokes Raman scattering microscopy," *Proc. Natl. Acad. Sci.* **100**, 9826–9830 (2003).
18. L. B. Mostaço-Guidolin et al., "Differentiating atherosclerotic plaque burden in arterial tissues using femtosecond CARS-based multimodal nonlinear optical imaging," *Biomed. Opt. Express* **1**, 59–73 (2010).
19. L.-J. den Hartigh et al., "Fatty acids from very low-density lipoprotein lipolysis products induce lipid droplet accumulation in human monocytes," *J. Immunol.* **184**, 3927–3936 (2010).
20. D. Débarre and E. Beaurepaire, "Quantitative characterization of biological liquids for third-harmonic generation microscopy," *Biophys. J.* **92**(2), 603–612 (2007).
21. R. R. Anderson, "Optical properties of human skin," in *The Science of Photomedicine*, pp. 147–194, Plenum Press, New York (1982).
22. G. Dobso, "Spectroscopy and spectrometry of lipids-part 1," *Eur. J. Lipid Sci. Tech.* **103**, 815–826 (2001).
23. M. Kratz et al., "Dietary mono- and polyunsaturated fatty acids similarly affect LDL size in healthy men and women," *J. Nutr.* **132**, 715–718 (2002).
24. I. H. Maliston, "Interspecimen comparison of the refractive index of fused silica," *J. Opt. Soc. Am.* **55**, 1205–1208 (1965).
25. R. B. Miles and S. E. Harris, "Optical third harmonic generation in alkali metal vapors," *IEEE J. Quantum Electron.* **9**(4), 470–484 (1973).
26. R. W. Boyd, *Nonlinear Optics*, Academic Press, Boston (1992).
27. Y. Barad et al., "Nonlinear scanning laser microscopy by third harmonic generation," *Appl. Phys. Lett.* **70**, 922–924 (1997).
28. G. O. Clay et al., "Spectroscopy of third-harmonic generation: evidence for resonances in model compounds and ligated hemoglobin," *J. Opt. Soc. Am. B* **23**, 932–950 (2006).
29. M. Müller et al., "3D microscopy of transparent objects using third-harmonic generation," *J. Microscopy* **191**, 266–274 (1998).
30. C.-F. Chang et al., "Direct backward third-harmonic generation in nanostructures," *Opt. Express* **18**(7), 7397–7406 (2010).
31. Y.-C. Chen et al., "Third-harmonic generation microscopy reveals dental anatomy in ancient fossils," *Opt. Lett.* **40**, 1354–1357 (2015).
32. F. F. de Sousa et al., "Dielectric properties of oleic acid in liquid phase," *J. Bionanosci.* **3**, 1–4 (2010).
33. S. A. Khodier, "Refractive index of standard oils as a function of wavelength and temperature," *Opt. Laser Tech.* **34**, 125–128 (2002).
34. C. Bosshard et al., "Non-phase-matched optical third-harmonic generation in non-centrosymmetric media: Cascaded second-order contributions for the calibration of third-order nonlinearities," *Phys. Rev. B* **61**(16), 10688–10701 (2000).
35. G. Veres et al., "Enhancement of third-harmonic generation in absorbing media," *Appl. Phys. Lett.* **81**(20), 3714–3716 (2002).
36. T. M. Liu et al., "Measuring plasmon-resonance enhanced third-harmonic $\chi^{(3)}$ of a Ag nanoparticles," *Appl. Phys. Lett.* **89**(4), 043122 (2006).
37. C. H. Yu et al., "Molecular third-harmonic-generation microscopy through resonance enhancement with absorbing dye," *Opt. Lett.* **33**(4), 387–389 (2008).
38. C. F. Chang, C. H. Yu, and C.-K. Sun, "Multi-photon resonance enhancement of third harmonic generation in human oxyhemoglobin and deoxyhemoglobin," *J. Biophoton.* **3**, 678–685 (2010).
39. M. R. Tsai et al., "Applying tattoo dye as a third-harmonic generation contrast agent for in vivo optical virtual biopsy of human skin," *J. Biomed. Opt.* **18**(2), 026012 (2013).
40. S. Y. Chen et al., "In vivo virtual biopsy of human skin by using noninvasive higher harmonic generation microscopy," *IEEE J. Sel. Top. Quant. Electron.* **16**(3), 478–492 (2010).
41. C. F. Chang et al., "Cell tracking and detection of molecular expression in live cells using lipid-enclosed cdse quantum dots as contrast agents for epi-third harmonic generation microscopy," *Opt. Express* **16**(13), 9534–9548 (2008).
42. P. Hourant et al., "Oil and fat classication by selected bands of near-infrared spectroscopy," *Appl. Spectrosc.* **54**, 1168–1174 (2000).
43. Y. R. Shen, *The Principles of Nonlinear Optics*, John Wiley & Sons, Inc., Hoboken, New Jersey (2003).
44. R. T. Holman and P.-R. Edmondson, "Near-infrared spectra of fatty acids and some related substances," *Anal. Chem.* **28**, 1533–1538 (1956).
45. R. F. Godou, "Determination of unsaturation by near-infrared spectrophotometry," *Anal. Chem.* **29**, 1790–1794 (1957).
46. H. Azizian et al., "Quantification of trans fatty acids in food products by GC, ATR-FTIR and FT-NIR methods," *Lipid Tech.* **16**, 229–231 (2004).
47. C. Molette et al., "The use of near-infrared reflectance spectroscopy in the prediction of the chemical composition of goose fatty liver," *Poult. Sci.* **80**, 1625–1629 (2001).
48. H. Li et al., "Rapid determination of cis and trans content, iodine value, and saponification number of edible oils by fourier transform near-infrared spectroscopy," *JAOCS* **76**, 491–497 (1999).
49. H. Li et al., "Trans determination of edible oils by fourier transform near-infrared spectroscopy," *J. Oil Fat Indus.* **77**(10), 1061–1067 (2000).
50. H. W. Wang et al., "Label-free bond-selective imaging by listening to vibrationally excited molecules," *Phys. Rev. Lett.* **106** (4), 238106 (2011).
51. J. Y. Lee et al., "Three-color multiplex CARS for fast imaging and microspectroscopy in the entire CHn stretching vibrational region," *Opt. Express* **17**, 22281–22295 (2009).
52. H. A. Rinia et al., "Quantitative label-free imaging of lipid composition and packing of individual cellular lipid droplets using multiplex CARS microscopy," *Biophys. J.* **95**, 4908–4914 (2008).
53. J. Squier et al., "Third harmonic generation microscopy," *Opt. Express* **3**, 315–324 (1998).
54. M. Zimmerley et al., "Probing ordered lipid assemblies with polarized third-harmonic-generation microscopy," *Phys. Rev. X* **3**, 011002 (2013).
55. H. B. de Aguiar, P. Gasecka, and S. Brasselet, "Quantitative analysis of light scattering in polarization-resolved nonlinear microscopy," *Opt. Express* **23**, 8960–8973 (2015).
56. P. D. Chowdary et al., "High speed nonlinear interferometric vibrational analysis of lipids by spectral decomposition," *Anal. Chem.* **82**(9), 3812–3818 (2010).

Yu-Cheng Chen received his MS degree in photonics and optoelectronics from National Taiwan University in 2012, and he worked as a research assistant in the Molecular Imaging Center until 2015. He is the author of more than 10 SCI journal publications, while his research

mainly focuses on plasmonics, nanophotonics, nonlinear optical microscopy, biophotonics, and ultrafast optics. Currently, he is studying his PhD in biomedical engineering at the University of Michigan, Ann Arbor.

Hsun-Chia Hsu received his BS and MS degrees in physics from National Taiwan University in 2008 and 2010, then he worked as a research assistant in the Molecular Imaging Center until 2013. His research mainly focuses on nonlinear optical effects, bioimaging, ultrafast optics, and photoacoustic microscopy. Currently, he is studying his PhD in biomedical engineering at Washington University in Saint Louis.

Chien-Ming Lee received his BS degree in optics and photonics from National Chiao Tung University in 2012. Since then, he joined his MS program in photonics and optoelectronics at National Taiwan University. His research mainly focuses on ultrafast spectroscopy, nonlinear optics, bioimaging, and theoretical calculations in ultrafast nonlinear optics.

Chi-Kuang Sun received his PhD in applied physics from Harvard University in 1995 and was an assistant researcher in the UCSB QUEST Center, from 1995 to 1996. In 1996, he joined National Taiwan University, where he is now a distinguished professor of photonics and optoelectronics. He founded the NTU Molecular Imaging Center. His research focuses on nano-acoustics, femtosecond optics, THz optoelectronics, and biomedical imaging. He is a fellow of OSA, SPIE, and IEEE.